Non-linear Finite Element Analysis of a Steel-concrete Composite Beam under Cyclic Loads Considering Interface Slip Effects

H. G. Kwak* and J. W. Hwang

Abstract— **This paper deals with an introduction of a numerical model to simulate bond-slip behavior in composite beams. The slip behavior is implemented into a finite element formulation and an adoption of the introduced numerical model makes it possible to take into account the slip behavior even in a beam element whose configuration is defined by both end nodes only. Correlation studies for bond-slip effect between numerical results were conducted, and a cyclic load-displacement relation of a composite beam is then evaluated to verify the validity of the proposed model.**

Index Terms—**Composite beams, Bond-slip, Non-linear analysis, Cyclic loads, Shear connectors**

I. INTRODUCTION

Composite bridges are constructed by placing a slab of concrete on a steel girder or a pre-cast concrete girder with shear connectors. The two components act as an integrated structure in spite of their very different physical and mechanical behaviors. In the design of composite beams, a very stiff shear connection between the beam and slab was provided usually. However, in partially composite beams having flexible shear connectors, the structural behavior becomes different greatly, as the slip between the beam and the slab accompanies a reduction of the strength and increase in the deflection.

To consider the slip behaviors described above, many studies have been carried out concerning partial shear connections. Some of previous methods [1], [2], [4], [5] give an exact solution for analyzing partially composite beams. However, only symmetric structures with zero slip at the midspan can be analyzed. To overcome these limitations, a few numerical models have been proposed. One study proposed a double node to represent the relative slip

between the steel beam and concrete slab [3]. The double node concept have been widely used and improved by many researchers. However, this method leads to an increase in the number of degrees of freedom and greater complexity in the mesh definition.

This paper, accordingly, introduces a finite element (FE) model which can include the bond-slip deformation in a beam element whose deformation is defined by two end nodes, without taking the double nodes along the interface between the concrete slab and beam. The reliability for the proposed model is verified by comparing the analytical predictions with results from previous analytical studies for bond-slip effects and by load-deflection curves of partially bonded and fully connected composite beams under cyclic loadings.

II. MATERIAL PROPERTIES

A. Concrete

Among the numerous mathematical models currently used in the analysis of RC structures, the monotonic envelop curve introduced by Kent and Park [7] and later extended by Scott et al. [13] is adopted in this paper because of its simplicity and computational efficiency for compressive region. More details related to the model can be found in [7] and [13]. On the other hand, it is assumed that concrete is linearly elastic in the tension region.

In case of hysteretic behavior, simplified model by Karsan and Jirsa [6] shown in Fig. 1 is adopted.
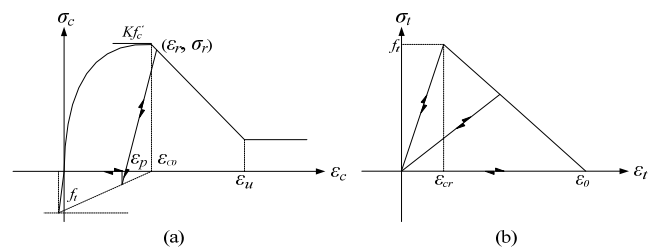

Fig. 1. Hysteretic stress-strain relation of concrete:
(a) compressive region; (b) tensile region

When unloading arises in the compressive area, the path passes through the point ε_t defined in Eq. (1) until it reaches the tensile strength.

$$\varepsilon_t = K\varepsilon_{c0}\{0.15(\varepsilon_r/K\varepsilon_{c0}) + 0.1(\varepsilon_r/K\varepsilon_{c0})^2\} \qquad (1)$$

Reaching the tensile strength, it drops to zero stress and keep unloading along the strain axis. When the path is reloaded before it reaches the tensile strength, it goes back along the unloading path. However, the path skips the wedge after it is reloaded after it reaches the tensile strength. The unloading pattern in the tensile area is similar with that in the compressive area except that it includes the tension stiffening effect. So every unloading stiffness value is different from each other by the point where unloading arises. For the simplicity, ε_{cr} is assumed to be same with ε_0 in this research.

B. Steel

The monotonic envelope of stress-strain relationship of steel was idealized as elasto-plastic behavior and the shape of the curve is assumed to be identical in the both of compressive and tensile area. At load reversals, as shown in Fig. 2, the unloading stiffness is assumed to be the same as the initial stiffness.
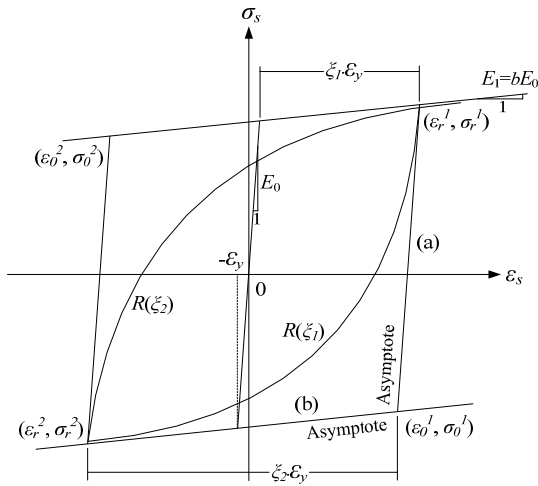

Fig. 2. Hysteretic stress-strain curve of steel

When loading continues in the opposite direction, the stress–strain curve exhibits the Bauschinger effect. This causes a non-linear stress–strain relation and a reduction in stiffness of the stress–strain curve before the stress reaches the yield stress in the opposite direction. Among a number of models developed to describe the cyclic stress–strain curve of reinforcing steel, the most commonly used approach is the Menegotto–Pinto model, introduced by Menegotto and Pinto. The model is also adopted in this paper and more details related to the model can be found in [10].

III. FORMULATION OF SLIP BEHAVIOR

A. Load-slip Relation

Since composite beams are equipped with shear connectors between a concrete slab and girder to unify the behavior of the total structure, the flexural and slip behavior of these composite beams are greatly influenced by the shear connectors characterized by their ductility and stiffness. Usually, the static behavior of shear connectors which govern the slip behavior at the interface can be explained through the shear stiffness in the elastic region, and the ultimate shear strength and the corresponding ultimate slip are measured by a push-out test.

In this research, a load-slip model by Salari and Spacone, as shown in Fig. 3, is adopted for the monotonic envelope. The monotonic envelope is divided into ascending and descending branches at the strength V_1 and more details can be found in [12]
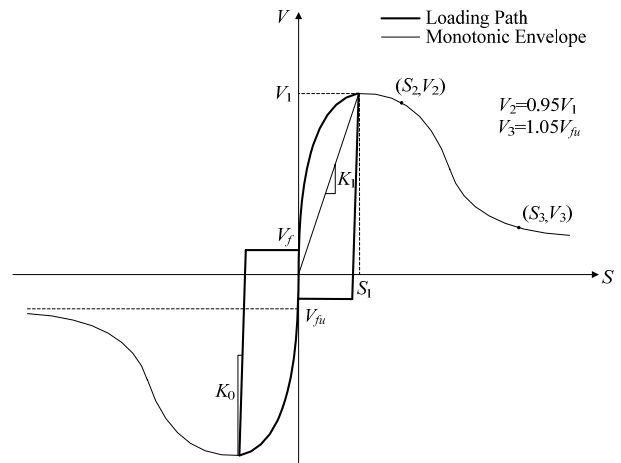

Fig. 3. Cyclic load-slip relation of a shear-stud

In case of unloading and reloading branch, not original complicated exponential model by Salari and Spacone but simplified by-linear formation is adopted in this research. When unloading arises, the loading path drops with its initial stiffness E_0 until it meets frictional resistant V_f and moves to monotonic envelope in the other side. Reloading path is assumed that it goes back in the same path of unloading path and reduced envelope by damage is not considered in this research.

And, if shear connectors are assumed to be installed under the uniform spacing L_s. the slip S can be represented by the following Eq. (2), where $q(x)$ is the shear force transmitted per unit length of the beam. This is known as the shear flow($q(x) = dF/dx$) F is horizontal force at the interface between two materials in coordinate x. which will be mentioned in the next chapter.

$$S = \frac{V(x)}{K_s} = \frac{q(x)L_s}{K_s} \tag{2}$$

B. Governing Equation for Slip Behavior

Fig. 4 shows the strain and corresponding stress distribution across the section of a composite beam with partial interaction. However, it will still be assumed that there is no separation between the two elements, which means the curvatures of two elements are identical.

The axial forces F and moments M act through the centroid of the concrete slab at a distance h_s from the slab–beam interface, as shown in Fig. 4(c), and at the centroid of the beam at a distance h_b from the interface. The elastic strains $\varepsilon_{s,b}$ at the bottom of the concrete slab and $\varepsilon_{b,t}$ at the top of the beam, as shown in Fig. 4(b), can be given from the beam theory by

$$\varepsilon_{s,b} = -\frac{F_s}{E_s A_s} + \frac{M_s h_s}{E_s I_s}, \quad \varepsilon_{b,t} = \frac{F_b}{E_b A_b} - \frac{M_b h_b}{E_b I_b} \tag{3}$$
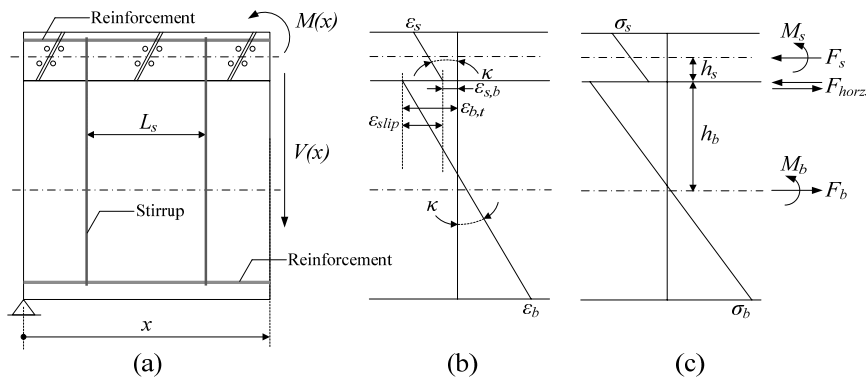
Fig. 4. Slip behavior in patially composite beam: (a) composite beam, (b) strains and curvature, (c) stresses and internal forces

where A_s and A_b are the areas of the concrete slab and beam respectively, while I_s and I_b are the moments of inertia of the cross-sectional area of each component with respect to their centroidal axes. Additionally, since there is no external longitudinal force being applied such as occurs in post-tensioning, horizontal force equilibrium requires that $\Sigma F = 0$ which implies that $F_s = F_b = F_{horz.}$

As mentioned above, when the composite section is subjected to the bending moment, the relative movement across the interface that is induced by the sliding action is referred to as the slip of $S = u_b - u_s$, and the derivative of this relation with respect to the longitudinal distance x gives the slip strain of $\varepsilon_{slip} = dS/dx = \varepsilon_{b,t} - \varepsilon_{s,b}$. Hence, from Eqs. (2) and (3), the following differential equation represented by the material constants and section dimensions can be obtained.

$$\frac{L_s}{K_s}\frac{d^2 F_{horz.}}{dx^2} = F_{horz.}\left[\frac{1}{E_s A_s} + \frac{1}{E_b A_b}\right] - \left[\frac{M_s h_s}{E_s I_s} + \frac{M_b h_b}{E_b I_b}\right] \quad (4)$$

From rotational equilibrium of the internal moment, the total moment $M(x)$ at the section being considered in Fig. 4(c) can be expressed by

$$M(x) = M_s(x) + M_b(x) + F(x)_{horz.}(h_s + h_b) \quad (5)$$

Since the shear connection is required to prevent separation between the beam and slab, the curvature κ in the slab and beam are the same, as shown in Fig. 4(b), so that

$$\kappa = \frac{M_s}{E_s I_s} = -\frac{1}{d_c}\left[\varepsilon_{s,t} - \varepsilon_{s,b}\right] \quad (6)$$

where d_c means the thickness of the concrete slab.

From Eqs. (5) and (6), the curvature κ at a section located at distance x from the far end support can be expressed by $\kappa = \{M(x) - F(x)_{horz.}(h_s + h_b)\}/\Sigma EI$, where $\Sigma EI = E_s I_s + E_b I_b$. In advance, Eq. (4) yields the following ordinary linear differential equation for $F(x)_{horz.}$

$$\frac{d^2 F(x)_{horz.}}{dx^2} - \frac{K_s}{L_s}\frac{EI^*}{EA^* \sum EI}F(x)_{horz.} = -\frac{K_s}{L_s}\frac{(h_b + h_s)}{(E_b I_b + E_s I_s)}M(x) \quad (7)$$

where $\dfrac{1}{EA^*} = \dfrac{1}{E_s A_s} + \dfrac{1}{E_b A_b}$, $EI^* = \sum EI + EA^*(h_s + h_b)^2$.

C. Numerical Slip Model

For computational convenience, the differential equation in Eq. (7) can be rewritten in the form of $F''(x) - P^2 F(x) = -QM(x)$, and the general solution of Eq. (7) representing $F(x)$ is obtained by summing a particular solution to the associated homogeneous solution, and the corresponding distribution of slip $S(x)$ is also obtained from the first derivation of the horizontal force. These lead to

$$F(x) = F_h + F_p = \alpha\cos(Px) + \beta\sinh(Px) + \frac{Q}{P^2}M(x) \quad (8)$$

$$S(x) = \frac{L_s}{K_s}\left(\frac{dF(x)}{dx}\right) = \frac{L_s}{K_s}\left\{\alpha P\sinh(Px) + \beta P\cosh(Px) + \frac{Q}{P^2}D(x)\right\}, \quad (9)$$

where $D(x)\ (= dM(x)/dx)$ means the slope of the moment distribution and gives a constant value if the distribution of moment $M(x)$ is assumed to be linear at each element, α and β are constants to be determined by substituting the boundary conditions at nodal points of each subdivided element.

In advance, the horizontal force $F(x)$ and the slip $S(x)$ at the interface of the concrete slab and beam, mentioned in Eqs. (8) and (9), can be represented in the ith element as the following matrix form:

$$\begin{Bmatrix} F_i(x) \\ S_i(x) \end{Bmatrix} = \begin{bmatrix} \cos(P_i x) & \sinh(P_i x) \\ T_i\sinh(P_i x) & T_i\cosh(P_i x) \end{bmatrix}\begin{Bmatrix} \alpha_i \\ \beta_i \end{Bmatrix} + \frac{Q_i}{P_i^2}\begin{Bmatrix} M_i(x) \\ \dfrac{L_{s,i}}{K_{s,i}}D_i \end{Bmatrix} \quad (10)$$

Where $T_i = (L_{s,i}/K_{s,i})\cdot P_i$ and l_i = the element length

Since the horizontal force and slip must maintain continuity along the entire span, those values at the common node i of the $(i-1)^{th}$ and i^{th} element must be the same, which means $F^i = F_{i-1}(l_{i-1}/2) = F_i(-l_i/2)$, $S^i = S_{i-1}(l_{i-1}/2) = S_i(-l_i/2)$ where F^i and S^i mean the horizontal force and corresponding sip at node i. Namely, the superscript i is assigned to all the parameters related to the node i. Substitution of above compatibility conditions and then rearrangement for the constant α and β, which will finally be determined, yield

$$\mathbf{A}_i = \mathbf{C}_{2,i}^{-1}\mathbf{C}_{1,i-1}\mathbf{A}_{i-1} + \mathbf{C}_{2,i}^{-1}\left[\mathbf{M}_{i-1} - \mathbf{M}_i\right] = \mathbf{C}_{2,i}^{-1}\mathbf{C}_{1,i-1}\mathbf{A}_{i-1} + \mathbf{C}_{2,i}^{-1}\Delta\mathbf{M}_i \quad (11)$$

where

$$\mathbf{A}_i = \begin{Bmatrix} \alpha_i \\ \beta_i \end{Bmatrix}, \quad \mathbf{A}_{i-1} = \begin{Bmatrix} \alpha_{i-1} \\ \beta_{i-1} \end{Bmatrix}, \quad \mathbf{M}_{i-1} = \frac{Q_{i-1}}{P_{i-1}^2}\begin{Bmatrix} M^i \\ \dfrac{L_{s,i-1}}{K_{s,i-1}}D_{i-1} \end{Bmatrix},$$

$$\mathbf{M}_i = \frac{Q_i}{P_i^2} \begin{Bmatrix} M^i \\ \dfrac{L_{s,i}}{K_{s,i}} D_i \end{Bmatrix},$$

$$\mathbf{C}_{1,i-1} = \begin{bmatrix} cosh(P_{i-1}\dfrac{l_{i-1}}{2}) & sinh(P_{i-1}\dfrac{l_{i-1}}{2}) \\ T_{i-1} sinh(P_{i-1}\dfrac{l_{i-1}}{2}) & T_{i-1} cosh(P_{i-1}\dfrac{l_{i-1}}{2}) \end{bmatrix}$$

$$\mathbf{C}_{2,i}^{-1} = \begin{bmatrix} cosh(-P_i\dfrac{l_i}{2}) & sinh(-P_i\dfrac{l_i}{2}) \\ T_i sinh(-P_i\dfrac{l_i}{2}) & T_i cosh(-P_i\dfrac{l_i}{2}) \end{bmatrix}^{-1} = \begin{bmatrix} cosh(P_i\dfrac{l_i}{2}) & \dfrac{1}{T_i}sinh(P_i\dfrac{l_i}{2}) \\ sinh(P_i\dfrac{l_i}{2}) & \dfrac{1}{T_i}cosh(P_i\dfrac{l_i}{2}) \end{bmatrix} \quad (12)$$

Since Eq. (11) refers to the vector of the solution coefficients of element i-1 and element i, successive application of this equation from the first element 1 to the last element n produces a generalized transfer matrix relationship, that express the relationship between the first element 1 and the element n, as

$$\mathbf{A}_n = \mathbf{C}_{2,n}^{-1}\left[\prod_{i=2}^{n-1}\mathbf{Z}_i\right]\mathbf{C}_{1,1}\mathbf{A}_1 + \sum_{i=2}^{n}\left\{\mathbf{C}_{2,n}^{-1}\left[\prod_{j=i}^{n-1}\mathbf{Z}_j\right]\Delta\mathbf{M}_i\right\} \quad (13)$$

where $\mathbf{Z}_i = \mathbf{C}_{1,i}\mathbf{C}_{2,i}^{-1}$ and $\prod_{i=2}^{n-1}\mathbf{Z}_i = \mathbf{Z}_{n-1}\cdot\mathbf{Z}_{n-2}\cdot\mathbf{Z}_{n-3}\cdots\mathbf{Z}_2$.

Two boundary conditions are required to solve Eq. (13). Since a multi-span continuous bridge usually has the simply supported boundary conditions at both far end points, which imply that the horizontal force and moment value are zero, the following boundary values can be introduced:

$$F^1 = F_1\left(-\frac{l_1}{2}\right) = 0, \qquad F^{n+1} = F_n\left(\frac{l_n}{2}\right) = 0 \quad (14)$$

$$M^1 = M_1\left(-\frac{l_1}{2}\right) = 0, \qquad M^{n+1} = M_n\left(\frac{l_n}{2}\right) = 0 \quad (15)$$

$$S^1 = S_1\left(-\frac{l_1}{2}\right), \qquad S^{n+1} = S_n\left(\frac{l_n}{2}\right) \quad (16)$$

In advance, substituting these boundary conditions into Eq. (10), the following relationships are obtained:

$$\mathbf{A}_1 = \begin{Bmatrix} \alpha_1 \\ \beta_1 \end{Bmatrix} = \mathbf{C}_{2,1}^{-1}\mathbf{D}_1 = \mathbf{C}_{2,1}^{-1}\begin{Bmatrix} 0 \\ S^1 - \dfrac{L_{s,1}}{K_{s,1}}\dfrac{Q_1}{P_1^2}D_1 \end{Bmatrix} = \mathbf{C}_{2,1}^{-1}\begin{Bmatrix} 0 \\ f(S^1) \end{Bmatrix} \quad (17)$$

$$\mathbf{A}_n = \begin{Bmatrix} \alpha_n \\ \beta_n \end{Bmatrix} = \mathbf{C}_{1,n}^{-1}\mathbf{D}_n = \mathbf{C}_{1,n}^{-1}\begin{Bmatrix} 0 \\ S^{n+1} - \dfrac{L_{s,n}}{K_{s,n}}\dfrac{Q_n}{P_n^2}D_n \end{Bmatrix} = \mathbf{C}_{1,n}^{-1}\begin{Bmatrix} 0 \\ f(S^{n+1}) \end{Bmatrix} \quad (18)$$

The substitution of Eqs. (17) and (18) into Eq. (13) produces the following system Eq. (19) related to the slip behavior at the interface of the slab and beam, and this equation can also be represented by matrix form of Eq. (20)

$$\mathbf{D}_n = \mathbf{G}\mathbf{D}_1 + \mathbf{H} \quad (19)$$

$$\begin{Bmatrix} 0 \\ f(S^{n+1}) \end{Bmatrix} = \begin{bmatrix} G_{11} & G_{12} \\ G_{21} & G_{22} \end{bmatrix}\begin{Bmatrix} 0 \\ f(S^1) \end{Bmatrix} + \begin{Bmatrix} H_1 \\ H_2 \end{Bmatrix} \quad (20)$$

Where $\mathbf{G} = \prod_{i=1}^{n}\mathbf{Z}_i = \mathbf{Z}_n\cdot\mathbf{Z}_{n-1}\cdots\mathbf{Z}_2\cdot\mathbf{Z}_1$ and $\mathbf{H} = \sum_{i=2}^{n}\left\{\left[\prod_{j=i}^{n}\mathbf{Z}_j\right]\Delta\mathbf{M}_i\right\}$.

In the matrix formulation of Eq. (20), the only unknowns are the slip values at the two far ends (S^1 and S^{n+1}) because all othecr values can be calculated from the coefficients of the governing equation and the nodal moment values. When the numerical model is applied to the non-linear problem, where stiffness of stud (K_s) is changed according to slip value, all the equations and expressions are changed into incremental form and all the values of variables in consideration should be evaluated by accommodating increments for any step, which is adopted in this research for the cyclic structural analysis.

IV. INTEGRATION WITH FE ANALYSIS

Numerical procedures of the bond-slip model mentioned at the previous chapter need to be modified appropriately to be unity with the discrete element system of a finite element analysis. Then, they can be implemented in a non-linear finite element method that uses Timoshenko beam elements [11] and the two analysis parts operate as one integrated analysis system. The evaluation procedures of the main variables of the bond-slip model are summarized as follows.

1) Coefficients of the governing equation (P_i, Q_i and $M_i(x)$) are computed.
2) The slip value S^1 at node 1 is computed.
3) Solution coefficients α_i and β_i of each element are computed.
4) The horizontal force F_{horz} and slip S of each element are computed.
5) The strain and stress distributions of the section of each element are determined, which become discontinuous due to the slip behavior.
6) The convergence is checked and iteration performed.

Step (5) is skipped after the 1st load increment because the equilibrium of horizontal force induced by the slip effect is considered in the procedure of finding two neutral axis of each component. Fig. 5 shows detail analysis procedure.

V. VERIFICATION

A. Slip Effects under Monotonic Loads

A total of three loading cases were tested. All beams are simply supported and have the same cross-sections and material properties. The first example was subjected to a uniformly distributed load of 25kN/m. The second example structure was subjected to a concentrated load of 9.8kN in the middle of the beam. The third example was also subjected to a concentrated load of 9.8kN, but the load was applied to the left quarter of the span ($L/4$). The length of the beam is 12m and the section dimensions are shown in Fig. 6.
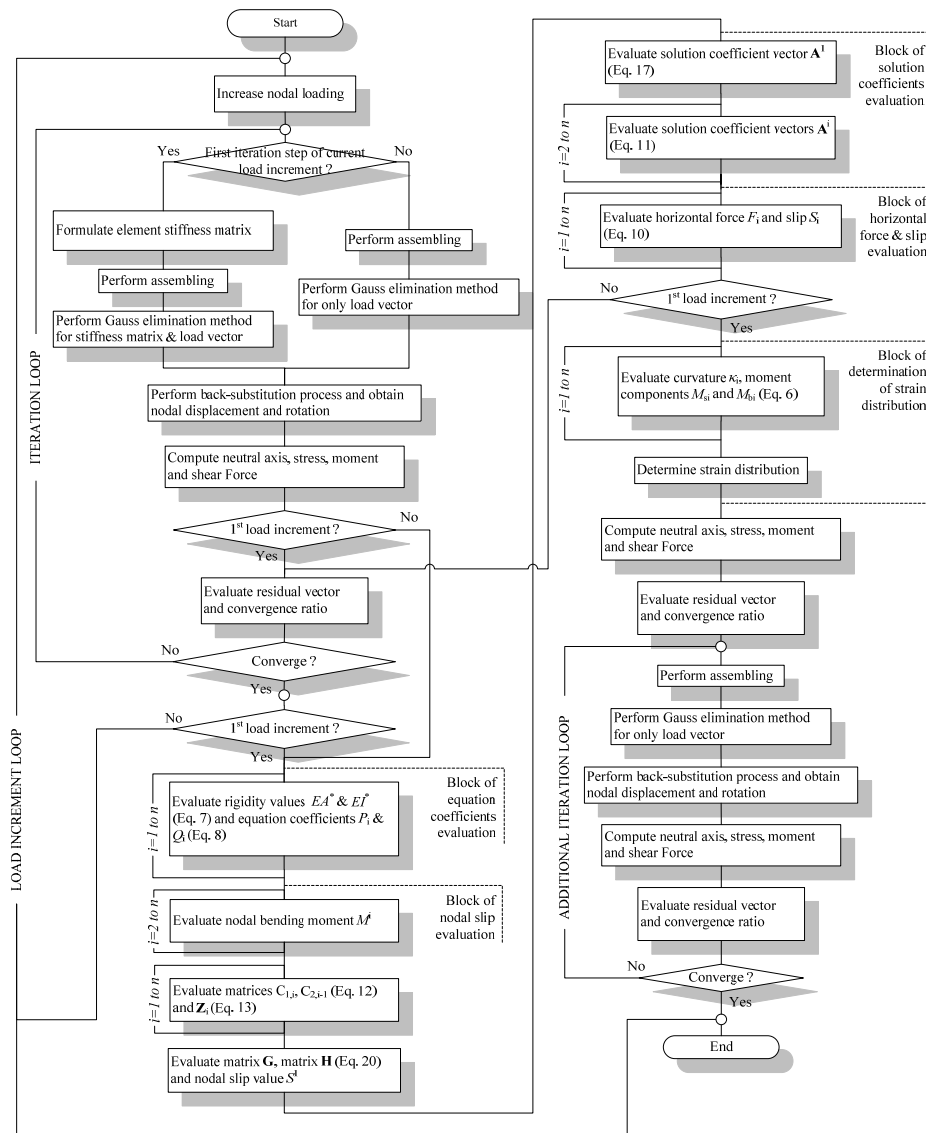
Fig. 5. Flow diagram of total analysis

The other material properties are listed in Table 1. The concrete slab is assumed to behave linearly up to its compressive strength, which is the same status with the earlier study [9] compared with this research.
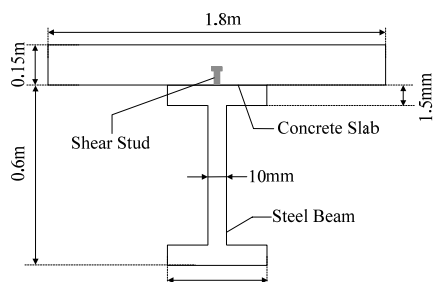

Fig. 6. Section dimensions of the steel-concrete composite beam

TABLE I
MATERIAL PROPERTIES OF STEEL-CONCRETE COMPOSITE BEAMS

K_s/L_s	E_c	E_s
150.0MPA	33.3GPA	200.0GPA

Fig. 7 shows the slip and horizontal force distributions of the structure, which was subjected to a few loading cases. The differences in all two types of curve between the model and the analytic calculation are scarcely noticeable even for the un-symmetric loading case, which show that the integrated model has no restriction in application to various structures subjected to arbitrary lateral loading.

B. Load-deflection Curves under Cyclic Loads

Non-linear F. E. analysis has been performed for the same steel composite beam, which is under cyclic load applied to midspan, and Table 2 includes material properties of shear studs used in the cyclic analysis.

TABLE II
MATERIAL PROPERTIES OF SHEAR STUDS

Initial bond stiffness	Ultimate bond force and corresponding slip	Bond-slip corresponding to $F_2 = 0.95$ F_1	Bond-slip corresponding to $F_3 = 1.05$ F_{fu}	Frictional bond resistance
$E_0 =$ 233000 kg/cm	$F_1 = 24000$ kg $S_1 = 0.225$ cm	$S_2 = 0.35$ cm	$S_3 = 2.0$ cm	$F_{fu} =$ 2500 kg $F_f = 400$ kg

Fig. 8 shows the load-deflection curves under cyclic load and two kinds of curves are plotted. One is the analysis results by applying the proposed bond-slip model and the other is analysis results by assuming perfect bond at the interface.
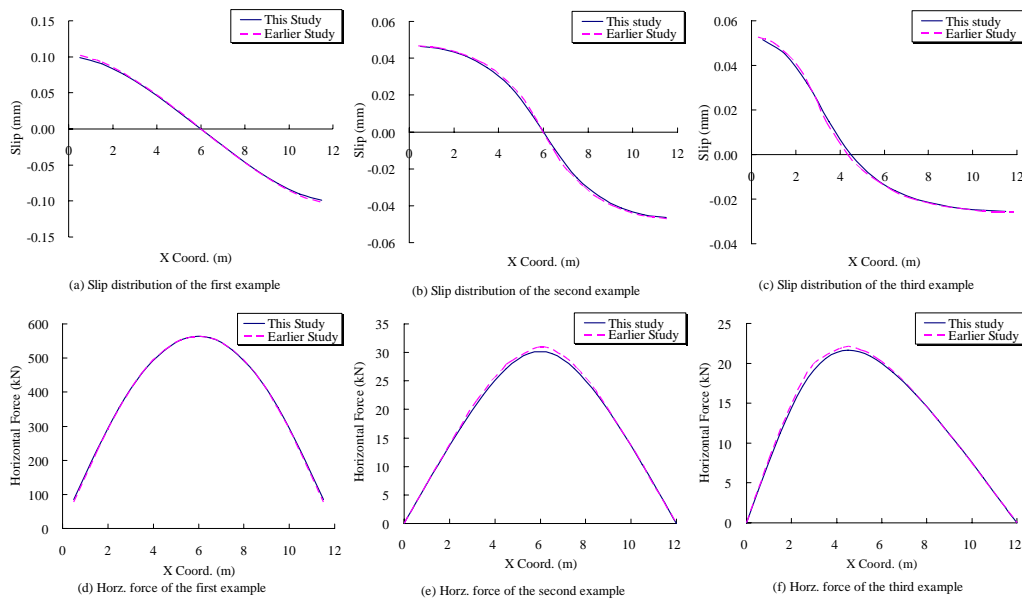
Fig. 7. Slip and horizontal force distributions of steel-concrete composite beams

Two curves show the both of convex and concave parts in a one unloading or reloading path caused by the asymmetry section resisting capacity, which means that the girder is fully composed of steel but the slab is composed of only concrete without any reinforcing. The partial bond case undergoes more severe deflection and, thus, it shows more flexible structural behavior than the perfect bond case, which is a very important characteristic of composite beams considering bond-slip effect. The difference of deflection becomes larger by increasing loads and it is very clear when the path in under large deflection.
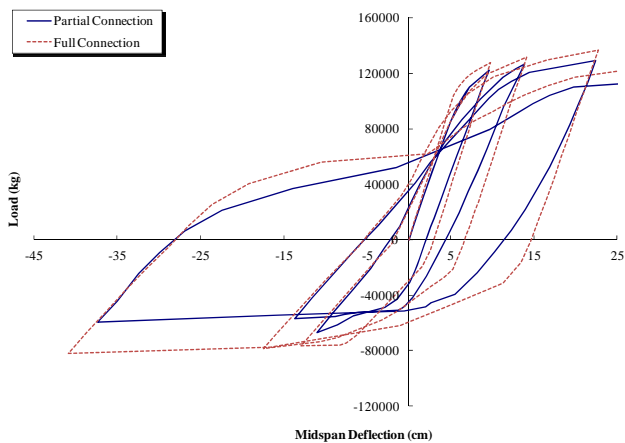

Fig. 8. Load versus mid-span deflection curves of a composite beam under cyclic loads

VI. CONCLUSION

In this paper, FE bond-slip model was introduced and it can perform structural analysis considering bond-slip effect with typical beam elements, which do not have to adopt double nodes. To establish the validity of the FE bond-slip model, a steel-concrete composite beam was used. The existing analysis results of the bond-slip model, as obtained from analytic calculation procedures, were compared with the analysis results of the FE bond-slip model and showed good agreement for the monotonic loading case for even an un-symmetric structure system. Verification was also extended for the cyclic loading conditions. Load-deflection curves obtained by the cyclic analysis shows the characteristics of bond-slip behavior in composite beams well.

REFERENCES

[1] Bradford, M.A. and Gilbert, R.I. (1992), "Composite beams with partial interaction under service loads", Journal of Structural Engineering, 118(10), 1871-1883.
[2] Dezi, L., Ianni, C. and Tarantino, A.M. (1993), "Simplified creep analysis of composite beams with flexible connectors", Journal of Structural Engineering, 119(5), 1484-1497.
[3] Gattesco, N. (1999), "Analytical modeling of non-linear behavior of composite beams with deformable connection", Journal of Constructional Steel Research, 52(2), 195-218.
[4] Jasim, N.A. and Atalla, A. (1999), "Deflections of partially composite continuous beams: A simple approach", Journal of Constructional Steel Research, 49(3), 291-301.
[5] Jasim, N.A. (1999), "Deflections of partially composite beams with linear connector density", Journal of Constructional Steel Research, 49(3), 241-254.
[6] Karsan, I.D. and Jirsa, J.O. (1969), Behavior of concrete under compressive loadings, Journal of Structural Division, 95(ST12), 2543-2563.
[7] Kent, D.C. and Park, R. (1971), "Flexural members with confined concrete", Journal of Structural Division, 97(ST7), 1969–1990.
[8] Kwak, H.G. and Filippou, F.C. (1990) Finite element analysis of reinforced concrete structures under monotonic loads, Report UCB/SEMM-90/14, Univ. of California, Berkely.
[9] Kwak, H.G. and Seo, Y.J. (2001), "Behaviour of steel-concrete composite beam with flexible shear stud", Proceedings of the Eighth International Conference on Civil and Structural Engineering Computing, Stirling.
[10] Menegotto, M. and Pinto, P.E. (1973), "Method of analysis for cyclically loaded reinforced concrete plane frame including changes in geometry and nonelastic behavior of elements under combined normal force and bending", Proceedings of IABSE symposium on resistance and ultimate deformability of structures acted on by well defined repeated loads, Lisbon.
[11] Owen, D.R.J. and Hinton, E. (1980), Finite elements in plasticity: theory and practice, Pineridge Press, Swansea.
[12] Salari, M.R. and Spacone, E. (2001), "Analysis of steel-concrete composite frames with bond-slip", Journal of Structural Engineering, 127(11), 1243-1250.
[13] Scott, B.D., Park, R. and Priestley, M.J.N. (1982), "Stress–strain behavior of concrete confined by overlapping hoops at low and high strain rates", ACI Structural Journal, 79(1), 13–27.
[14] Welch, G.B. and Haisman, B. (1969), Fracture toughness measurements of concrete, Report No. R42, Univ. of New South Wales, Sydney.